Performance of the MISR LAI and FPAR Algorithm

A Case Study In Africa

Jiannan Hu[1], Bin Tan[1], Nikolay Shabanov[1], Katheen A. Crean[2], John V. Martonchik[2],

Dave J. Diner[2], Yuri Knyazikhin[1], and Ranga B. Myneni[1]

[1]Department of Geography, Boston University, Boston, MA 02215, USA

[2]Multi-angle Imaging Element, Jet Propulsion Laboratory

Correspondence

Jiannan Hu

Department of Geography

Boston University

675 Commonwealth Avenue

Boston, MA 02215, USA

Telephone: 617-353-8845

Fax: 617-353-8399

Email: jiannan@bu.edu

Submitted for publication in
Remote Sensing of Environment

Distributed by the Atmospheric Science Data Center
http://eosweb.larc.nasa.gov

Abstract

The multi-angle imaging spectroradiometer (MISR) instrument is designed to provide global imagery at nine discrete viewing angles and four visible/near-infrared spectral bands. The MISR standard products include vegetation green leaf area index (LAI) and fraction of photosynthetically active radiation absorbed by vegetation (FPAR). These parameters have been routinely processed at the Langley ASDC since October 2002. This paper presents a research related to the transition of the MISR LAI/FPAR product from the beta to the provisional status. The quality and spatial coverage of the MISR Land Surface Reflectances input to the algorithm determine the quality and spatial coverage of the LAI and FPAR products. Considerable efforts, therefore, has been expended to analyze the performance the algorithm as a function of uncertainties in the MISR surface reflectances. An additional goal of the MISR LAI/FPAR algorithm is the classification of vegetation in terms of biome types, a parameter that usually is specified as an input for other LAI/FPAR algorithms that use single-angle observations. It was shown that the use of multi-angle data allows the algorithm to minimize the biome misclassification when this has a significant effect on LAI retrievals. As a result, with a high probability, uncertainties in LAI retrievals due to the biome misclassification do not exceed uncertainties in observations. Considerable attention was also paid to characterizing the quality of the LAI/FPAR parameters and this information is available to the users as quality assessment indicators accompanying the product. Inspection and analysis of the MISR LAI/FPAR product demonstrate that the successfully retrieved LAI and FPAR values follows regularities expected from physics. The provisional LAI/FPAR algorithm realizes the basic principle of retrieval techniques, i.e., the more information that's available and

Distributed by the Atmospheric Science Data Center
http://eosweb.larc.nasa.gov

the more accurate this information is, the more reliable and accurate the algorithm output will be. Improvements to the quality of the land surface reflectances, therefore, will automatically lead to better quality of LAI and FPAR retrievals.

INTRODUCTION

The multi-angle imaging spectroradiometer (MISR) is an instrument on board the EOS-Terra platform. MISR makes global observations of the Earth's surface at 1.1 km spatial resolution with the objective of determining the atmospherically corrected reflectance properties of most of the land surface and the tropical ocean (Martonchik et al., 1998). The basic land surface parameters currently being generated at the NASA Langley Atmospheric Science Data Center (ASDC) include the spectral hemispherical-directional reflectance factor (HDRF) at the nine MISR view angles and the associated bihemispherical reflectance (BHR). The hemispherical directional reflectance factor (HDRF) and the bihemispherical reflectance (BHR) characterize surface reflectance under ambient sky conditions, i.e., direct and diffused illumination. The bidirectional reflectance factor (BRF) and the directional hemispherical reflectance (DHR) are defined for the unique case when the atmosphere is absent. An algorithm to produce vegetation green leaf area index (LAI) and fraction of photosynthetically active radiation absorbed by vegetation (FPAR) from BHR and BRF (Knyazikhin et al., 1998) become operational in October 2002. An additional goal of the MISR LAI/FPAR algorithm is the classification of vegetation in terms of biome types, a parameter that usually is specified as an input for other LAI/FPAR algorithms that use single-angle observations. In this paper, we provide an analysis of the performance of the provisional MISR LAI/FPAR algorithm.

Distributed by the Atmospheric Science Data Center
http://eosweb.larc.nasa.gov

The quality and spatial coverage of BHR and BRF determine the quality and spatial coverage of the LAI and FPAR products. Therefore, we start with the description of MISR data and an analysis of uncertainties in the MISR surface reflectances followed by a discussion of some of the spatial scaling issues associated with the MISR LAI/FPAR algorithm. A special attention is given to analyze the performance the algorithm as a function of uncertainties in the MISR BHR and BRF as well as to develop indicator flags characterizing the retrieval quality.

MISR DATA

The MISR data distributed from the NASA Langely Atmospheric Sciences Data Center were used in this study. The MISR data are in the format of path (swath) and orbit. About 233 paths cover the earth; each path is about 360 km wide from East to West. The orbit marks the path data from different dates.

The MISR Level 2 Surface Parameters Product contains information on land surface directional reflectance properties, albedos, both spectral and PAR integrated, FPAR, associated radiation parameters and terrain referenced geometric parameters. These data, in HDF format and at 1.1 km spatial resolution, are the source of BRFs, HDRFs, DHRs and BHRs (expansion of abbreviation is given in a list at the beginning of this article).

The view angles at the surface for each of the nine MISR cameras, as well as the incident solar angle at the surface are contained in the MISR Geometric Parameters Product. This information is at a spatial resolution of 17.6 km, and is an input to the LAI/FPAR algorithm. The latitude and longitude information is contained in the MISR Ancillary Geographic Product (MISR Interface Control Document).

Distributed by the Atmospheric Science Data Center
http://eosweb.larc.nasa.gov

An at launch MODIS six-biome map, was used to identify the pixel biome type. The six biomes are grasses and cereal crops, shrubs, broadleaf crops, savannas, broadleaf forests and needleleaf forests. The upper-left and bottom-right latitude and longitude of the MISR data block are used as georeferences to reproject the biome map to MISR SOM-j projection.

MISR data from Africa were selected for this investigation as in situ LAI and FPAR measurements were available from several sites in Southern Africa (Privette et al., 2001; Tian et al., 2002). These field data, although collected in 2000, are valuable for estimating certain algorithm parameters, as will be detailed elsewhere in this article. In particular, we concentrate our analysis on Southern Africa and MISR data from March 2001 - the earliest period for which the MISR LAI/FPAR products are available.

The repeat cycle of MISR coverage is 9 days. But in view of cloud cover, data from an entire month are required to obtain full coverage of Southern Africa. Assembling the data set in this fashion meant that we were assuming minimal canopy changes during this month, and this will introduce uncertainty in the derived results. This uncertainty will be assessed during the course of this investigation.

The moderate spatial resolution, multispectral and multiangle aspects of MISR imply large data volumes and hence the need for analysis stratified by biome type. Raw data, which were corrupted or with incorrect geometry information (negative angles) were excluded from analysis. Likewise, invalid reflectance data, for example, BHRs greater than 1, were ignored. A schematic of the data processing is shown in Fig. 1.

The MISR data from path 162 to 203 were used in this study and these cover Africa. The ratio of pixels with valid data to the total number of pixels is shown in Fig. 2, separately for different biomes. In general, the data from each path are from different days. About 42% of the pixels

Distributed by the Atmospheric Science Data Center
http://eosweb.larc.nasa.gov

contain valid data, useful as inputs to the algorithm. This number changes by date and by biome type, and may be as low as 36% in the case of broadleaf forests, where cloud cover is persistent.

DATA ANALYSIS

The nominal view angles for the nine cameras are 0.0, +/- 26.1, +/- 45.6, +/- 60.0 and +/- 70.5 (in degrees). The variation in actual view angles relative to the specification, for the fore and aft off-nadir sensors, is presented in Fig. 3. The maximum deviation in view zenith angles is for camera A fore and aft (4.95 and 4.84 degrees) respectively. This deviation decreases with increasing view zenith angle. Most of the deviations are positive, reasons for which are not known. These variations contribute to uncertainty in the LAI/FPAR retrievals.

Uncertainties in land surface reflectance determine the quality of LAI and FPAR retrievals (Wang et al, 2001). Calibration and processing for atmospheric effects of the measured radiance induce uncertainties in the surface reflectance products. Land surface reflectance parameters, HDRF and BHR, are inputs of the LAI/FPAR algorithm. Therefore, the uncertainties in MISR surface reflectance product are evaluated below.

MISR surface reflectance data are first sorted according to biome type. Data density distribution functions, defined as the number of pixels per unit area in the red-NIR space, are evaluated for each biome type. Pixels located around the data peak, i.e. the maximum pixel number, can be interpreted as the set of pixels representing the most probable pattern of canopy structure. As an example, the data density distribution function for broadleaf forests is shown in Fig. 4a. These pixels are selected for further analysis.

The mean and standard deviation of the HDRFs and BHRs are shown in Figs. 4b-d, for different biomes. Uncertainties in HDRFs are larger at large view angles (except the A camera),

Distributed by the Atmospheric Science Data Center
http://eosweb.larc.nasa.gov

and greater for the near-infrared channel in comparison to the red channel except the uncertainties in angle nine (standard deviations in Red band for the nine view angles, from angle 1 to angle 9 are 0.031, 0.019, 0.015, 0.016, 0.016, 0.014, 0.013, 0.019, 0.042; standard deviations in NIR band for the nine view angles are 0.033, 0.026, 0.024, 0.023, 0.024, 0.019, 0.017, 0.022, 0.040). The uncertainties are generally similar in the fore and aft angles. The BHR magnitudes with respect to biome type, shown in Fig. 4d, display expected behavior. In the red channel, shrubs are brighter and the BHR magnitude decreases with increasing tree cover. In the near-infrared, the opposite is seen. Although the uncertainties are generally comparable at both wavelengths, they are considerably larger in the red channel on a relative basis (uncertainties in Red band is 0.0055, 0.0054, 0.0055, 0.0056, 0.0029 for the five biomes respectively versus uncertainties in NIR band of 0.0056, 0.0055, 0.0056, 0.0056, 0.0056).

The uncertainties in Figs. 4b-d may result from variations in view angles (for HDRF), variation in vegetation canopy structure and due to atmosphere correction. Deviation from nominal view zenith angle certainly impacts the HDRF values, because the HDRF is view angle dependent. But, such uncertainties are likely to be small because view angle variations were small (Fig. 3).

Vegetation cover type mixture may also contribute to uncertainties in reflectance data. Variations in canopy structure due to biome mixtures are minimized by selecting pixels around the data peak. These pixels may be considered representative of a biome type with minimal mixing. Therefore, uncertainties due to biome mixture are unlikely to cause the variations seen in Figs. 4b-d.

Thus uncertainties in input BHR and HDRF remain even after excluding the minor uncertainties due to variations in MISR view zenith angle, cover type mixtures and further assuming minimal biome classification error. Such intrinsic uncertainties may be the most significant uncertainties of

Distributed by the Atmospheric Science Data Center
http://eosweb.larc.nasa.gov

the MISR surface reflectance product. There may be due to atmospheric correction, and this is further investigated in the following temporal analysis.

In this method, we assume the vegetation structure to remain unchanged during the month of March. The coefficients of variation (standard deviation divided by the mean) in Blue, Red, and NIR bands from three different days from path 178 are shown in Fig.5 for different biomes. The histogram is widely scattered especially in the blue band of grasses/cereal crops and broadleaf forests, which is likely due to correction for atmospheric effects. Likewise, the histograms are broad at the red band, especially in the case of broadleaf forests. The most probable value of the coefficient of variation is least for the NIR band (about 0.15 for grasses/cereal crops, about 0.4 for broadleaf forests).

Only three different days of data were available in March and it is clear that this sample is insufficient to analyze a random variable, especially to characterize its standard deviation. At least in the case of broadleaf forests, the LAI does not change much during the peak green season. Therefore, variation in canopy structure can be excluded for this cover type. The large uncertainties here may be due to errors in pixel geolocation, or may be due to atmospheric correction.

From the comparison presented in Fig. 6, between the uncertainties derived from spatial analysis and temporal analysis, it is obvious that uncertainties from the temporal analysis are greater than the uncertainties from spatial analysis for most biome types, with the exception of shrubs, where both kinds of uncertainties are similar in both bands. The uncertainties of the temporal analysis are significant and they are taken as the upper bounds in our LAI/FPAR retrievals.

Distributed by the Atmospheric Science Data Center
http://eosweb.larc.nasa.gov

SCALING OF THE ALGORITHM

In the MISR LAI/FPAR algorithm, the three-dimensional radiative transfer equation is used to simulate canopy reflectances as a function of biome type, sun-view geometry and canopy/soil patterns. Global vegetation is stratified into six canopy architectural types or biomes in this approach to LAI/FPAR retrievals. The structural attributes of these biomes are parameterized in terms of variables that the radiative transfer equation admits (Myneni et al., 1997). The six biomes are grasses and cereal crops, shrubs, broadleaf crops, savannas, broadleaf forests and needleleaf forests. The transport equation was adjusted to model canopy reflectances of the six biome types at 30 m spatial resolution, which is taken as the reference resolution. However, when the spatial resolution of the imagery becomes significantly coarser than 30 m, both the degree of biome mixing within a pixel and the number of mixed pixels in the imagery increases. An investigation of the effect of land cover mixtures within a pixel shows that LAI retrieval errors are inversely related to the proportion of the dominant land cover type in the pixel if the within pixel heterogeneity is not accounted by the retrieval technique (Tian et al, 2002a and 2002b). Errors are particularly large when forests are minority biomes in non-forest pixels compared to when forest biomes are mixed with one another, and vice-versa. Thus, the retrieval algorithm must be adjustable, to allow for spatial scale effects. Here we follow a technique developed by Tian et al (2002c), which accounts for pixel heterogeneity through modifications to the single scattering albedo that the radiative transfer equation admits through the use of land cover fractions.

To specify appropriate values for the single scattering albedo, the MISR DHRs corresponding to the peak green season are located in the red-NIR spectral space for each of the biome types (Fig. 4a). Pixels located around the data peak can be interpreted as the set of pixels representing the most

Distributed by the Atmospheric Science Data Center
http://eosweb.larc.nasa.gov

probable pattern of canopy structure. Neglecting contribution of the surface underneath the canopy, the most probable value of DHR at wavelength λ is related to canopy transmittance and absorptance at this wavelength as

$$1-\mathrm{DHR}_{\lambda}=\frac{q}{1-\omega_{\lambda}p_{t}}+\frac{1-\omega_{\lambda}}{1-\omega_{\lambda}p_{i}}(1-q)\,. \tag{1}$$

Here ω_λ is the single scattering albedo defined as the ratio of energy scattered by the elementary volume formulated for the radiative transfer equation, to energy intercepted by this volume; q is the probability that a photon in the incident radiation will arrive at the bottom of the canopy without suffering a collision (uncollided radiation), $\omega_\lambda p_t$ and $\omega_\lambda p_i$ are portions of collided radiation in total radiation transmitted and intercepted by the vegetation canopy, respectively (Shabanov et al., 2002; Wang et al., 2002). The wavelength independent parameters q, p_t, and p_i are functions of LAI. Equation (1) expresses the energy conservation law, namely, radiation absorbed by a vegetated surface (the left-hand side) is the sum of radiant energy absorbed by the underlying surface and vegetation (the first and second terms on the right-hand side of equation (1), which are the canopy transmittance, $t_{bs,\lambda}$, and absorption calculated for the case of a black surface underneath the canopy). In the case of a reflecting Lambertion surface, the term $\frac{\rho_\lambda}{1-\rho_\lambda r_{s,\lambda}} t_{s,\lambda} t_{bs,\lambda}$ should be subtracted from the left-hand side of equation (1) to account for the contribution of the ground to the canopy leaving radiation (see equation (41) in Knyazikhin et al, 1998). Here ρ_λ is the reflectance of the underlying surface; $t_{s,\lambda}$ and $r_{s,\lambda}$ are fractions of radiation transmitted and

Distributed by the Atmospheric Science Data Center
http://eosweb.larc.nasa.gov

reflected by the vegetation canopy if it were illuminated from below by an isotropic source (Knyazikhin et al, 1998).

Leaf area index values corresponding to the most probable canopy realization must be known in order to calibrate the algorithm, and this is usually accomplished through field measurements. Given biome type and LAI, as well as measured DHR_λ, and modeled q, p_t and p_i corresponding to this LAI value, the algorithm is then adjusted for data resolution by finding values of the single scattering albedo ω_λ which provide the best agreement between the left and right sides of equation (1). Values of DHR for Africa, obtained from MISR retrievals (1-23 March 2001) and field measurements made during the SAFARI 2000 wet season campaign (3-18 March 2000) and the Operation Canopy La Makande'99 campaign (2-10 March 1999) (Panferov et al, 2001), were used to scale the LAI/FPAR algorithm to the MISR resolution. A MODIS biome classification map was used to sort the MISR DHR data into individual biome classes. The spectral ground reflectance ρ_λ is assumed to vary within given biome-dependent ranges representative of reflective properties of the most probable surfaces underneath the canopy (Knyzikhin et al, 1998).

The above method is followed to scale MISR LAI/FPAR algorithm. The most probable data, which have the minimal variations in vegetation structure, are used as the input data. Figure 7a shows locations of the most probable values of (1- DHR_λ) at red and NIR wavelengths, for different biomes. The algorithm is adjusted for data resolution by finding values of the single scattering albedo which provide the best agreement between the retrieved and measured LAI values. The solutions to this problem are shown in Fig. 7b. These single scattering albedos are used by the operational MISR LAI/FPAR software. Fig. 7c shows histograms of LAI retrievals for grasses & cereal crops and broadleaf forests, which are centered at about 1.5 and 5.0, respectively. These mean values agree well with LAI measured in the field (Myneni et al, 2002; Privette et al, 2002).

Distributed by the Atmospheric Science Data Center
http://eosweb.larc.nasa.gov

PERFORMANCE OF THE ALGORITHM AS A FUNCTION OF UNCERTAINTIES

At least two types of uncertainties influence the quality of retrievals uncertainties in the land surface reflectance product and in the model used to simulate surface reflectance. In general, these uncertainties set a limit to the quality of retrievals; that is, accuracy in the retrievals cannot be better than summary accuracy in data and the model. If uncertainties are ignored, it can result not only in the loss of information conveyed by the algorithm, but also can result in its destabilization (Wang et al., 2001). Thus, the use of uncertainty information in the retrieval technique can influence the quality of retrievals. An overall uncertainty in model and measurements is input to the MISR LAI/FPAR retrieval technique (Knyazikhin et al., 1998). The aim of this section is to empirically estimate an upper limit of acceptable uncertainties in data and observations which provides optimal performance of the algorithm.

Let A_k and $r_{k,i}$, k=1, 2, …,4, i=1,2, …, 9, be atmospherically corrected BHRs at four spectral bands and BRFs at four spectral bands and in 9 MISR directions, respectively. We treat these values as independent random variables with finite variances $\sigma_A(k)^2$ and $\sigma_r(k,i)^2$ k=1, 2, …,4, i=1,2, …, 9, and assume that the deviations $\varepsilon_k = (A_k - \overline{A}_k)/\sigma_A(k)$ and $\delta_{k,i} = (r_{k,i} - \overline{r}_{k,i})/\sigma_r(k,i)$ follow Gaussian distributions. Here $\overline{A}_k$ and $\overline{r}_{k,i}$ are the mathematical expectations of A_k and $r_{k,i}$ which are treated as "true values." The random variables

$$\chi_{\mathrm{A}}^2 = \sum_{k=1}^{N_{\mathrm{bands}}} \varepsilon_k^2 = \sum_{k=1}^{N_{\mathrm{bands}}} \frac{(A_k - \overline{A}_k)^2}{\sigma_A(k)^2}, \qquad (2)$$

Distributed by the Atmospheric Science Data Center
http://eosweb.larc.nasa.gov

$$\chi_r^2 = \sum_{i=1}^{N_{\text{view}}} \sum_{k=1}^{N_{\text{bands}}} \delta_{k,i}^2 = \sum_{i=1}^{N_{\text{view}}} \sum_{k=1}^{N_{\text{bands}}} \frac{(r_{k,i} - \bar{r}_{k,i})^2}{\sigma_r(k,i)^2}, \tag{3}$$

characterizing the proximity of atmospherically corrected data to true values have chi–square distributions. Here N_{bands} and N_{view} are numbers of spectral bands and view directions for which the MISR observations are available. Inequalities $\chi_A^2 \le N_{\text{bands}}$ and $\chi_r^2 \le N_{\text{bands}} N_{\text{view}}$ indicate good accuracy in the atmospherically corrected surface reflectances with a high probability. Dispersions $\sigma_A(k)$ and $\sigma_r(k,i)$ are uncertainties in the land surface reflectance product which are input to the MISR LAI/FPAR algorithm. Model uncertainties, $\sigma_{A,\text{m}}(k)$ and $\sigma_{r,\text{m}}(k,i)$ can be defined in a similar manner (Wang et al., 2001). Note that currently the MISR algorithm uses two spectral bands, red and NIR (N_{bands}=2) to retrieve LAI and FPAR.

Overall uncertainties in BHR, $\delta_A(k)$, and BRF, $\delta_r(k,i)$ which guarantee the convergence property of the retrieval technique (i.e., increasingly accurate retrievals with increasingly accurate inputs) can be represented as $\delta_A(k)^2 = [\sigma_A(k)^2 + \sigma_{A,\text{m}}(k)^2]/\theta_A^2$, $\delta_r(k,i)^2 = [\sigma(k,i)^2 + \sigma_{r,\text{m}}(k,i)^2]/\theta_r^2$. Here stabilization parameters θ_A and θ_r vary between 0.5 and 1 (Wang et al., 2001). To evaluate proximity of observed to modeled surface reflectances, true values $\bar{A}_k$, $\bar{r}_{k,i}$, and uncertainties in the surface reflectance product $\sigma_A(k)$ and $\sigma_r(k,i)$ that appear in equations. (2) and (3) should be substituted with modeled reflectances and overall uncertainties (Wang et al., 2001). We assume that the model uncertainties do not exceed uncertainties in observations; that is, $\sigma_{A,\text{m}}(k)/\sigma_A(k) < 1$ and $\sigma_{r,\text{m}}(k,i)/\sigma(k,i) < 1$. The overall uncertainties in BHR and BRF can be represented as $\delta_A(k) = (\alpha_A/\theta_A)\sigma_A(k)$ and $\delta_r(k,i) = (\alpha_r/\theta_r)\sigma_r(k,i)$, respectively. Here the coefficients α_A and α_r vary between 1 and 2. A correct specification of the ratios $\gamma_A = (\alpha_A/\theta_A)$ and $\gamma_r = (\alpha_r/\theta_r)$, each varying between 1 and 4, are required to derive LAI and FPAR of the highest possible quality (Wang et al.,

Distributed by the Atmospheric Science Data Center
http://eosweb.larc.nasa.gov

2001). Based on the above arguments, we will evaluate upper bounds of γ_A and γ_r which provide optimal performance of the algorithm. Standard deviations derived from spatial analysis (Figs. 4b-d) are taken as lower bounds of uncertainties in the observations.

The MISR algorithm retrieves LAI and FPAR values using a two-step process. The first step involves a comparison of the MISR BHR with those determined from a suite of canopy models, which depend on biome type, canopy structure, and soil/understory reflectances. All canopy, soil and biome patterns for which modeled and observed BHRs at the four spectral bands differ by an amount equivalent to or less than the uncertainty in model and observations are considered as acceptable solutions. FPAR is also calculated for each acceptable solution. For each biome pattern *bio*, *bio* = 1, 2, ... , 6, the algorithm then evaluates mean $\mathrm{LAI}_1(bio)$ and $\mathrm{FPAR}_1(bio)$ over acceptable solutions, their dispersions, $\Delta\mathrm{LAI}_1(bio)$, $\Delta\mathrm{FPAR}_1(bio)$, and number $N_{\mathrm{sol},1}(bio)$ of acceptable solution. Equation (2) with overall uncertainties in modeled and observed BHRs is used to execute the first step. The biome, canopy, and soil patterns that pass this comparison test are subject to the second step, which is comparison of directional signatures of modeled and observed BRFs. And again, for each biome type, mean $\mathrm{LAI}_2(bio)$ over acceptable solutions, its dispersion, $\Delta\mathrm{LAI}_2(bio)$ and number $N_{\mathrm{sol},2}(bio)$ of acceptable solutions are evaluated. Equation (3) with appropriate overall uncertainties is used to execute the second test. For each 1.1 km MISR pixel within which BHR/BRF retrieval was performed, $\mathrm{LAI}_1(bio)$, $\Delta\mathrm{LAI}_1(bio)$, $N_{\mathrm{sol},1}(bio)$, $\mathrm{LAI}_2(bio)$, $\Delta\mathrm{LAI}_2(bio)$, and $N_{\mathrm{sol},2}(bio)$, *bio*=1,2,...,6, are archived in the Aerosol/Surface Product. The FPAR is evaluated and archived for each 17.6 km region.

An additional goal of the MISR LAI/FPAR algorithm is the classification of vegetation in terms of biome types described in the previous section, a parameter that usually is specified as an input for other LAI/FPAR algorithms that use single-angle observations. Based on the output

Distributed by the Atmospheric Science Data Center
http://eosweb.larc.nasa.gov

archived, the following biome identification algorithm will be examined here. Assuming that more than one of the candidate biomes passes the second test (the comparison of retrieved and modeled directional reflectances), the biome type with the minimum coefficient of variation ($\Delta LAI_2/LAI_2$) of LAI (COVLAI) is chosen as being most representative of the observed vegetation type. If the same minimum COVLAI is found for more than one biome type, then the biome type with the smallest mean LAI is chosen. If this process fails to identify a unique biome type, the retrieval is classified as unsuccessful.

An analysis presented earlier has showed that uncertainties in the surface reflectances can be quite high (Figs. 4 and 5). Figure 2 shows availability of valid MISR surface reflectances which, on average, constitute 42% of the vegetated land for the selected paths. A subset of these surface reflectances whose uncertainties exceed a certain acceptable level will result in algorithm failure, reducing the number of successful LAI and FPAR retrievals. This number can be increased by setting the ratios γ_A and γ_r to higher values. The retrieval quality, however, will decrease in this case. A decrease in γ_A and γ_r will result in fewer successful retrievals. It should be emphasized that this does not necessarily improves the retrieval quality. In general, the underestimation of the overall uncertainties can result in lower retrieval quality than their overestimation (Wang, 2001). Our aim here is to evaluate optimal values of γ_A and γ_r which allow the algorithm to discriminate between pure biome types, to minimize the impact of biome misidentification on LAI retrievals, and to maximize the number of successful retrievals.

Two variables are used to characterize the algorithm performance as a function of uncertainties. The first, is the retrieval index (RI), defined as the ratio between the number of retrieved LAI values and the total number of pixels with valid surface reflectance data. This variable does not characterize the retrieval quality, but shows the spatial coverage of the retrieved

Distributed by the Atmospheric Science Data Center
http://eosweb.larc.nasa.gov

LAI and FPAR fields. The second, is the biome identification index (BI), the ratio of the number of cases for which the algorithm correctly identifies the biome type to the number of successfully retrieved pixels.

The following procedure was executed to specify optimal values of the overall uncertainties. For each biome type, pixels located around the data peak were selected (Fig. 4a). Given values of the ratios γ_A and γ_r for each biome type, the MISR LAI/FPAR algorithm was executed using these surface reflectances and the six-biome map described earlier. Next, from the initial set of pixels we select those that passed the first and/or second compression tests. A Quality indicator of the Algorithm (QA) is assigned to each pixel, indicating that a retrieval passed both comparison tests (QA=0, highest quality), the first test only (QA=1, intermediate quality), or the second test only (QA=2, low quality). The RI as a function of QA and biome type is also calculated. The biome identification algorithm is then applied to the new set of pixels and the BI as a function of QA is calculated. Within this procedure, the RI is the conditional probability of retrieving a LAI value given biome type, while the BI is the probability to identify the biome type. By calculating RI(γ_A,γ_r,*bio*,QA) and BI(γ_A,γ_r,*bio*,QA) for all possible combinations of the ratios γ_A and γ_r, one selects those which result in the maximum to the following performance index (PI),

$$PI(bio) = \sum_{QA=0}^{2} RI(\gamma_A, \gamma_r, bio, QA) \cdot BI(\gamma_A, \gamma_r, bio, QA) . \tag{4}$$

In this procedure, relative values $\nu_A(k,bio) = \delta_A(k,bio)/A_k$ and $\nu_r(k,i,bio) = \delta_r(k,bio)/r_{k,i}$ were used to parameterize the overall uncertainties in the model and observations. Given relative uncertainties,

Distributed by the Atmospheric Science Data Center
http://eosweb.larc.nasa.gov

the MISR LAI/FPAR algorithm approximates actual overall uncertainties as $\delta_A(k,bio) = \nu_A(k,bio)A_k$ and $\delta_r(k,i,bio) = \nu_r(k,i,bio)r_{k,i}$ which are taken as acceptable levels of uncertainties.

Figures 8a-c show RI(bio,QA), BI(bio,QA) and PI(bio,QA) for the optimal set of relative overall uncertainties whose values are listed in Tables 1 and 2. With the expectation of broadleaf crops, the algorithm retrieves LAI values with a very high probability, if information about the biome type is available and uncertainties in input do not exceed the acceptable level. The probability of identifying pure biome types is quite high if both tests were successfully executed with the exception of broadleaf crops and savannas (Fig. 8b, bars labeled "QA=0"). If uncertainties in BRFs exceed the acceptable level and, as a consequence the second test fails, the probability of identifying grasses/cereal crops, shrubs, savannas and broadleaf forests based on BHRs only is greatly reduced (Fig. 8b, bars labeled "QA=1"). The first comparison test tends to extract information about canopy structure conveyed by the location of biome type in the spectral space. Although the locations of pure biome types in the spectral space are localized (Fig. 4d), the uncertainties in BHRs do not allow the algorithm to take full advantages of this property. Their effect is most pronounced in the case of spectrally similar biomes like broadleaf crops and savannas (Fig. 4d). Thus, the inclusion of additional angular information can compensate for the loss of information due to uncertainties in input surface reflectances. Values of the BI corresponding to QA=2 are higher compared to those derived from the first test only, with the exception of broadleaf crops (QA=1). This suggests that the angular signature of vegetation conveys more information about the canopy structure than the location of BHRs in the spectral space, at least, for the data investigated here. However, as will be shown later in this paper, the use of BRFs only result in a lower retrieval quality, as compared to when the first test only or both tests are triggered to retrieve LAI values. This is because an increase in the amount of angular

Distributed by the Atmospheric Science Data Center
http://eosweb.larc.nasa.gov

information not only increases the information content but also decreases the overall accuracy in the data. The former enhances quality of the retrievals, while the latter suppresses it. A failure of the algorithm to execute the first test indicates high uncertainties in BHR which, propagating through the surface retrieval algorithm, result in a poor quality of BRF and, as a consequence, LAI retrievals. At the Langley ASDC, the operational version of the algorithm generates LAI and FPAR products only for the conditions of QA=0 and QA=1, i.e., the first or both comparison tests must be passed.

IMPACT OF BIOME MISIDENTIFICATION ON LAI RETRIEVALS

Figure 8c shows the PI for six biome types. On average, for only about 20% of pixels, both LAI and biome type can be simultaneously specified at the optimal level of uncertainties. It means that the majority of LAI values are retrieved using incorrect information about biome type. Table 3 summarizes disagreement between the biome types derived from the MISR LAI/FPAR algorithm and the six-biome map described earlier as a function of QA. For given vegetation type, a distribution of biomes assigned by the MISR algorithm is shown in rows. The aim of this section is to analyze the impact of biome misidentification on LAI retrievals. In other words, what is impact of biome misidentification on LAI retrievals.

To address this question we compare two LAI fields. The first one, produced by the algorithm using the biome map as input, is taken as a reference field. The second LAI field was obtained by applying the MISR LAI/FPAR algorithm to the same data set without using information on biome type. For each pixel for which both retrievals were available, a relative difference, Δ, between reference, LAI_{ref}, and retrieved, LAI_{MISR}, values was calculated, i.e.,

Distributed by the Atmospheric Science Data Center
http://eosweb.larc.nasa.gov

$$\Delta = \frac{LAI_{ref} - LAI_{MISR}}{LAI_{ref}}. \tag{5}$$

Pixels located around biome dependent data peaks (Fig. 4a) were used to generate these values. Figure 9 shows histograms of Δ as a function of QA for different biome types. Mean values and standard deviations of the relative difference Δ are shown in Table 4. With the expectation of shrubs and broadleaf crops, the impact of biome misidentification on LAI retrievals is minimal if both comparison tests were executed.

Histogram of Δ for shrubs corresponding to QA=1 has two local minimums at $\Delta = 0$ and $\Delta =$ -0.7. This biome was mainly misclassified as broadleaf forests and needle forests (Table 3). Reference and retrieved LAI values for which the relative difference was close to -0.7 varied around 0.2 and 0.34, respectively. Shrubs exhibit lateral spatial heterogeneity, low to intermediate vegetation ground cover, and bright background. The information conveyed about the canopy structure is small and a wide range of natural variation in ground cover and soil can result in the same value of the BHR. Broadleaf and needle forests with a very low ground cover and bright understory can results in similar values of surface reflectances at 1.1 km resolution. The effects of biome misclassification on the retrievals, therefore, is maximal if retrievals passed the first test only (curve "QA=1" in Fig. 9b). Availability of additional angular information results in a reduced disagreement between reference and retrieved LAI values (curve "QA=0" in Fig. 9b). Note that the probability of identifying shrubs using angular information only (QA=2) is very high (see Figure 8b and Table 3). However, the inclusion of LAI retrievals corresponding to QA=2 has no significant effect on the PI (see Eq. (4) and Fig. 8a). Note that a failure of the algorithm to execute

Distributed by the Atmospheric Science Data Center
http://eosweb.larc.nasa.gov

the first test (QA=2) indicates high uncertainties in BHR which, propagating through the surface retrieval algorithm, result in a poor quality of BRF, and, as a consequence, LAI retrievals.

For other biome types, a disagreement between reference and retrieved LAI values are maximal for QA=2 (Table 4). If retrievals passed the first or both comparison tests, the biome misidentification, on average, involves an underestimation of LAI values for grasses/cereal crops and shrubs, and an overestimation in the case of broadleaf crops, savannas and broadleaf forests (see Fig. 9 Table 4). In general, misclassification between distinct biomes has a significant effect on LAI retrieval. For example, shrubs are mainly misclassified as broadleaf or needle forests (see Table 3, QA=1). The mean relative difference is –0.37 compared to –0.14 when the probability of such a misidentification is much lower (see Table 3, QA=0).

What is the probability that biome misidentification has no impact on LAI retrieval? To address this question, we introduce the most probable relative difference as values of Δ at which its histogram achieves its local maximums. One can see from Fig. 9 that many of histograms have two local maximums. However, all biomes have a local maximum around $\Delta = 0$. Table 5 lists most probable values $\overline{\Delta}$ and probabilities of $|\Delta - \overline{\Delta}| \leq \chi$ for different biome types, QA values and disagreement level χ.

For grasses/cereal crops, shrubs, savannas and broadleaf forests, the disagreement between reference and high quality retrievals (QA=0) does not exceed 15% with probabilities 97%, 68%, 71% and 99%, respectively (Table 5). For 81% of savannas, the relative difference corresponding to QA=0 and $\overline{\Delta}$=0 is about 25%. With the expectation of shrubs, more than 70% of intermediate quality retrievals agree with reference values to within 25%. For these retrievals, however, probabilities of $|\Delta| \leq 0.25$ are reduced. On average, with a probability of 70% and higher, the high and intermediate quality retrievals agree with true values to within 25% uncertainties which is close

Distributed by the Atmospheric Science Data Center
http://eosweb.larc.nasa.gov

to an overall uncertainty in model and observations (see Tables 1 and 2). Thus, the optimal performance of the algorithm minimizes the biome misclassification when it has a significant effect on LAI retrievals. With a very high probability, uncertainties due to the biome misclassification do not exceed uncertainties in model and observations.

Note that a biome type is an important input parameter to LAI/FPAR algorithms that use single-angle observations. A typical overall accuracy in biome maps is about 70% (Lotsch et al., 2002) and thus about 30% of LAI retrievals should be treated as unreliable. Pixels impacted by the biome misclassification are difficult to identify. The use of angular and spectral signatures of vegetations instead of biome map allows us not only to obtain comparable accuracy, but also to assign quality flags to retrievals. It should also be noted that uncertainties in the reference LAI field are unknown and thus the above analyses do not characterize uncertainties in retrievals. However, proximity of the retrieved to the reference LAI field indicates that angular and spectral signatures of vegetation provide a sufficient amount of information needed to retrieve LAI values without using land cover maps as input.

It is well known that there is a strong relationship between a vegetation index, such as NDVI, and surface parameters such as LAI and FPAR (Asrar et. al., 1984; Tucker and Sellers, 1986; Peterson et. al. 1987; Verma et. al. 1993; Myneni and Williams, 1994; Chen, 1996). This relationship provides a method to test the physics of retrievals. NDVI values were regressed against both LAI and FPAR to ascertain whether the proper relationships were obtained. The NDVI values were computed using the MISR nadir view HDRF values in the red and NIR bands. It should be emphasized that the LAI values were determined using the MISR algorithm and MISR surface reflectances as inputs without using the NDVI. Fig. 10 shows the NDVI-LAI and NDVI-FPAR regression curves for grasses and broadleaf forests, based on the MISR data. High quality retrievals

Distributed by the Atmospheric Science Data Center
http://eosweb.larc.nasa.gov

(QA=0) were used to derive these curves. The biome specific relationships between retrieved LAI/FPAR and NDVI conform to both theoretical and empirical expectations. Fig. 11 shows NDVI-LAI relationships for grasses/cereal crops and broadleaf forests corresponding to different values of QA. One can see that curves corresponding to QA=2 do not follow regularities expected from physics and are mainly outside of the error bars of curves the NDVI-LAI relationships derived from high quality retrievals. A failure of the algorithm to execute the first test (QA=2) indicates high uncertainties in BHR which, propagating through the surface retrieval algorithm, result in a poor quality of BRF, and, as a consequence, LAI retrievals. At the Langley ASDC, the operational version of the algorithm will generate LAI and FPAR products only for the condition of QA=0 and QA=1.

CONCLUDING REMARKS

The algorithm to retrieve biophysical parameters (LAI, FPAR, biome type) from MISR BHR and BRF have been routinely processed at the Langley ASDC since October 2002. This paper presents a research related to the transition of the MISR LAI/FPAR product from the beta to the provisional status. The quality and spatial coverage of the MISR Land Surface Reflectances input to the algorithm determine the quality and spatial coverage of the LAI and FPAR products. Therefore, our primary objective is to establish the convergence of the MISR LAI/FPAR algorithm; that is, the more the measured information and the more accurate this information is, the more reliable and accurate the algorithm output will be.

Uncertainties in model and measurements are input to the MISR LAI/FPAR retrieval technique. An upper limit of acceptable uncertainties in the MISR surface reflectances which

Distributed by the Atmospheric Science Data Center
http://eosweb.larc.nasa.gov

allows the algorithm to discriminate between pure biome types, to minimize the impact of biome misidentification on LAI retrievals, and to maximize the spatial coverage of retrievals was empirically evaluated. Surface reflectances whose uncertainties exceed the acceptable level of 20% result in algorithm failure, reducing the number of successful LAI and FPAR retrievals. The data analysis indicates that uncertainties in the MISR BHR of dense vegetations at red and blue spectral bands can substantially exceed the acceptable level. At these wavelengths, dense vegetations exhibit low reflectances. As it is indicated in the Statement Concerning Quality of MISR Level 2 Aerosol/Surface Products (version v2.2_i4), reliability of land surface retrievals can be low in this case. High uncertainties in BHR retrievals over dark vegetation, therefore, can result in algorithm failure, reducing the number of successful retrievals.

On average, for about 20% of pixels, both LAI and biome type can be simultaneously specified at the current level of uncertainties in the MISR surface reflectance product. About 80% of LAI values are retrieved using incorrect information about biome type. However, the LAI/FPAR algorithm minimizes the biome misclassification when it has a significant effect on LAI retrievals. With a probability of about 70%, uncertainties in LAI retrievals due to the biome misclassification do not exceed uncertainties in observations.

Considerable attention was also paid to characterizing the quality of the LAI/FPAR parameters and this information will be available to the users as quality assessment indicators accompanying the product. A Quality indicator of the Algorithm (QA), being used with LAI/FPAR retrievals in the current study, takes on values between 0 and 2, indicating that a retrieval passed both comparison tests (QA=0, highest quality) the first test only (QA=1, intermediate quality), or the second test only (QA=2, low quality). An analyses presented in this paper indicates that, with a high probability, the quality indicator correctly reflects retrieval quality. Based our investigation,

Distributed by the Atmospheric Science Data Center
http://eosweb.larc.nasa.gov

one can conclude that the LAI/FPAR algorithm realizes the basic principle of any retrieval technique, i.e., the more information that's available and the more accurate this information is, the more reliable and accurate the algorithm output will be. Improvements to the quality of the Land Surface reflectances, therefore, will lead to better quality of LAI and FPAR retrievals.

ACKNOWLEDGEMENTS

We thank the Langley Research Center (LaRC) DAAC (The NASA Distributed Active Archive Centers) providing the MISR data.

Distributed by the Atmospheric Science Data Center
http://eosweb.larc.nasa.gov

REFERENCES

Asrar, G., M. Fuchs, E. T. Kanemasu, and J. L. Harfield. (1984). Estimating absorbed photosynthetic radiation and leaf area index from spectral reflectance in wheat, Agron. J., 76, 300-306.

Chen, J. M. (1996). Canopy architecture and remote sensing of the fraction of photosynthetically active radiation absorbed by boreal conifer forests. *IEEE Transaction on Geoscience and Remote Sensing*, 34, 1353–1368.

Diner, D. J., Beckert, J. C., Reilly, T. H., Bruegge, C. J., Conel, J. E., Kahn, R. A., Martonchik, J. V., Ackerman, T. P., Davies, R., Gerstl, S. A. W., Gordon, H. R., Muller, J. P., Myneni, R. B., Sellers, P. J., Pinty, B., and Verstraete, M. M. (1998). Multi-angle Imaging SpectroRadiometer (MISR) instrument description and experiment overview. *IEEE Transaction on Geoscience and Remote Sensing*, 36, 1072-1087.

Knipling, E. B. (1969). Leaf reflectance and image formation on color infrared film. In: P. O. Johnson, *Remote sensing in ecology* (pp. 17-19). University Georgia Press, Athenes, Georgia.

Knyazikhin, Y., Martonchik, J.V., Diner, D.J., Myneni, R.B., Verstraete, M., Pinty, B., and Gobron, N. (1998). Estimation of vegetation canopy leaf area index and fraction of absorbed photosynthetically active radiation from atmosphere-corrected MISR data. *Journal of Geophysical Research*, 103, 32239-32256.

Lotsch, A., Tian, Y., Friedl, M. A., and Myneni, R. B. (2001). Land cover mapping in support of LAI and FAPAR retrievals from EOS-MODIS and MISR: Classification methods and sensitivities to errors. *International. Journal of Remote Sensing*, (accepted for publication).

Distributed by the Atmospheric Science Data Center
http://eosweb.larc.nasa.gov

Myneni, R. B., Nemani, R. R. and Running, S. W. (1997). Estimation of Global Leaf Area Index and Absorbed Par Using Radiative Transfer Models. *IEEE Transaction on Geoscience and Remote Sensing*, 35, 1380-1393.

Myneni, R. B., Hoffman, S., Knyazikhin, Y., Privette, J.L., Glassy, J., Tian, Y., Wang, Y., Song, X., Zhang, Y., Smith, G.R., Lotsch, A., Friedl, M., Morisette, J.T., Votava, P., Nemani, R. R., and Running, S.W. (2002). Global products of vegetation leaf area and fraction absorbed PAR from year one of MODIS data. *Remote Sensing of Environment*, 83, 214-231.

Myneni, R. B., & Williams, D. L. (1994). On the relationship between FAPAR and NDVI. *Remote Sensing of Environment.* 49, 200–211.

Panferov, O., Knyazikhin, Y., Myneni, R. B., Szarzynski, J., Engwald, S., Schnitzler, K. G., and Gravenhorst, G. (2001). The Role of Canopy Structure in the Spectral Variation of Transmission and Absorption of Solar Radiation in Vegetation Canopies. *IEEE Transaction Geoscience.and Remote Sensing*, 39(2), 241-253.

Peterson, D. L., Spanner, M. A., Running, R. W., & Band, L. (1987). Relationship of thematic mapper simulator data to leaf area index. *Remote Sensing of Environment*, 22, 323–341.

Privette, J.L., Myneni, R.B., Knyazikhin, Y., Mukelabai, M., Roberts, G., Tian, Y., Wang, Y., and Leblanc, S.G. (2002). Early spatial and temporal validation of MODIS LAI product in the southern Africa Kalahari. *Remote Sensing of Environment*, 83, 232-243

Privette, J. L., Myneni, R. B., Roberts, M. G. (2001). Validation of the MODIS LAI product in an African woodland. *Remote Sensing of Environment*, (submitted for publication).

Shabanov, N.V., Wang, Y., Buermann1, W., Dong, J., Hoffman, S., Smith, G.R., Tian, Y., Knyazikhin, Y., and Myneni, R.B. (2002). Validation of the Radiative Transfer Principles of

Distributed by the Atmospheric Science Data Center
http://eosweb.larc.nasa.gov

the MODIS LAI/FPAR Algorithm with Data from the Harvard Forest. *Remote Sensing of Environment*, (submitted for publication).

Tian, Y., Wang, Y., Zhang, Y., Knyazikhin, Y., Bogaert, J., and Myneni, R. B. (2001). Radiative Transfer Based Scaling of LAI/FPAR Retrievals From Reflectance Data of Different Resolutions. *Remote Sensing of Environment*, 84, 143-159.

Tian, Y., Woodcock, C. E., Wang, Y., Shabanov, N. V., Privette, J. L., Zhou, L., Knyazikhin, Y., Veikkanen, B., Hame, T., Buermann, W., Dong, J., Ozdogan, M. and Myneni, R. B. (2002a). Multiscale analysis and validation of MODIS LAI product over Maun, Botswana. I. Uncertainty Assessment. *Remote Sensing of Environment*, 83, 414-430.

Tian, Y., Woodcock, C. E., Wang, Y., Shabanov, N. V., Privette, J. L., Zhou, L., Knyazikhin, Y., Veikkanen, B., Hame, T., Buermann, W., Dong, J., Ozdogan, M. and Myneni, R. B. (2002b). Multiscale analysis and validation of MODIS LAI product over Maun, Botswana. II. Sampling Strategy. *Remote Sensing of Environment*, 83, 431-441.

Tucker, C. J., & Sellers, P. J. (1986). Satellite remote sensing of primary production. *International Journal of Remote Sensing*, 7, 1395–1416.

Wang, Y., Tian, Y., Zhang, Y., El-Saleous, N., Knyazikhin, Y., Vermote, E., Myneni, R. B. (2001). Investigation of product accuracy as a function of input and model uncertainties Case study with SeaWiFS and MODIS LAI/FPAR algorithm. *Remote Sensing of Environment* 78:299-313.

Wang, Y., Buermann, W., Stenberg, P., Smolander, H., Häme, T., Tian. Y., Hu. J., Knyazikhin, Y., Myneni, R. B. (2002). Hyperspectral Remote Sensing of Vegetation Canopy Leaf Area Index and Foliage Optical Properties. *Remote Sensing of Environment*, (submitted for publication).

Distributed by the Atmospheric Science Data Center
http://eosweb.larc.nasa.gov

Verma, S. B., Sellers, P. J., Walthall, C. L., Hall, F. G., Kim, J., & Goetz, S. J. (1993). Photosynthesis and stomatal conductance related to reflectance on the canopy scale. *Remote Sensing of Environment*, 44, 103–116.

Distributed by the Atmospheric Science Data Center
http://eosweb.larc.nasa.gov

Table 1. Optimal values of relative uncertainties, ν_A, in modeled and observed BHRs.

Biome Type	Grass and Cereal Crops	Shrubs	Broadleaf Crops	Savanna	Broadleaf Forests
Red	0.2	0.08	0.15	0.4	0.2
NIR	0.05	0.05	0.05	0.1	0.2

Table 2. Optimal values of relative uncertainties, ν_r, in modeled and observed BRFs.

View Angle	Spectral band	Grass and Cereal Crops	Shrubs	Broadleaf Crops	Savanna	Broadleaf Forests
nadir	Red	0.2	0.2	0.15	0.2	0.15
	NIR	0.2	0.2	0.05	0.2	0.05
Aa, Af	Red	0.2	0.15	0.15	0.2	0.15
	NIR	0.2	0.05	0.05	0.2	0.05
Ba, Bf	Red	0.2	0.2	0.225	0.2	0.225
	NIR	0.2	0.2	0.075	0.2	0.075
Ca, Cf	Red	0.2	0.2	0.3	0.2	0.3
	NIR	0.2	0.2	0.1	0.2	0.1
Da, Df	Red	0.2	0.2	0.45	0.2	0.45
	NIR	0.2	0.2	0.15	0.2	0.15

Distributed by the Atmospheric Science Data Center
http://eosweb.larc.nasa.gov

Table 3. Disagreement between biome types assigned by the MISR algorithm and the six biome classification map used in the study for different values of QA.

Landcover Type	QA	Landcover Type assigned by MISR algorithm, %						
		Grasses/Cereal Crops	Shrubs	Broadleaf Crops	Savannas	Broadleaf Forests	Needleleaf Forests	Failure
Grasses/Cereal Crops	0	81	7	4	1	0	0	7
	1	5.49	39.47	14.06	0	0	0	40.98
	2	29.94	14.48	0.08	0	8.5	35.19	11.81
Shrubs	0	0.03	38.33	0.91	0.01	13.91	3.37	43.44
	1	0	20	0	0	32	11	37
	2	0	100	0	0	0	0	0
Broadleaf Crops	0	n/a	n/a	n/a	n/a	n/a	n/a	n/a
	1	0	2	69	0	0	29	0
	2	4	11	16	0.02	18	26	25
Savannas	0	42.7	3.3	9.5	37.2	0	6.7	0.6
	1	26	20	31	15	0	7	1
	2	n/a	n/a	n/a	n/a	n/a	n/a	n/a
Broadleaf Forests	0	0	0	0	0	100	0	0
	1	0	0	0	77.5	12.5	0	10
	2	3.9	8.8	9.6	0	16	42.1	20

Table 4. Mean values and standard deviations of the relative difference for different biome type and QA.

	Mean			Standard Deviation		
	QA=0	QA=1	QA=2	QA=0	QA=1	QA=2
Grasses & Cereal Crops	-0.01	-0.13	0.20	0.05	0.10	1.68
Shrubs	-0.14	-0.37	0	0.29	0.34	0.00
Broadleaf Crops	n/a	0.45	0.60	n/a	0.73	3.03
Savannas	0.17	0.05	n/a	0.76	0.68	n/a
Broadleaf Forests	0	0.04	-0.35	0	0.05	0.22

Distributed by the Atmospheric Science Data Center
http://eosweb.larc.nasa.gov

Table 5. Most probable values $\overline{\Delta}$ of the relative difference Δ and probabilities of $|\overline{\Delta}-\Delta|<\chi$ for different biome types, QA and disagreement level χ.

	Most Probable Value			Prob $(|\overline{\Delta}-\Delta|<\chi)$					
	QA=0	QA=1	QA=2	QA=0		QA=1		QA=2	
				$\chi=0.15$	$\chi=0.25$	$\chi=0.15$	$\chi=0.25$	$\chi=0.15$	$\chi=0.25$
Grasses & Cereal Crops	0	-0.1	0	0.97	0.99	0.86	0.96	0.44	0.51
Shrubs	0	0	0	0.68	0.68	0.32	0.32	1	1
	-0.7	-0.7	-	0.32	0.32	0.68	0.68	-	-
Broadleaf Crops	-	0	0	-	-	0.71	0.71	0.6	0.71
	-	0.4	-	-	-	0.04	0.04	-	-
	-	1.7	-	-	-	0.25	0.25	-	-
Savannas	0	0	-	0.71	0.81	0.57	0.7	-	-
	-0.6	-0.6	-	0.06	0.06	0.22	0.22	-	-
Broadleaf Forests	0	0	0	1	1	1	1	0.2	0.3
	-	-	-0.45	-	-	-	-	0.5	0.66

Distributed by the Atmospheric Science Data Center
http://eosweb.larc.nasa.gov

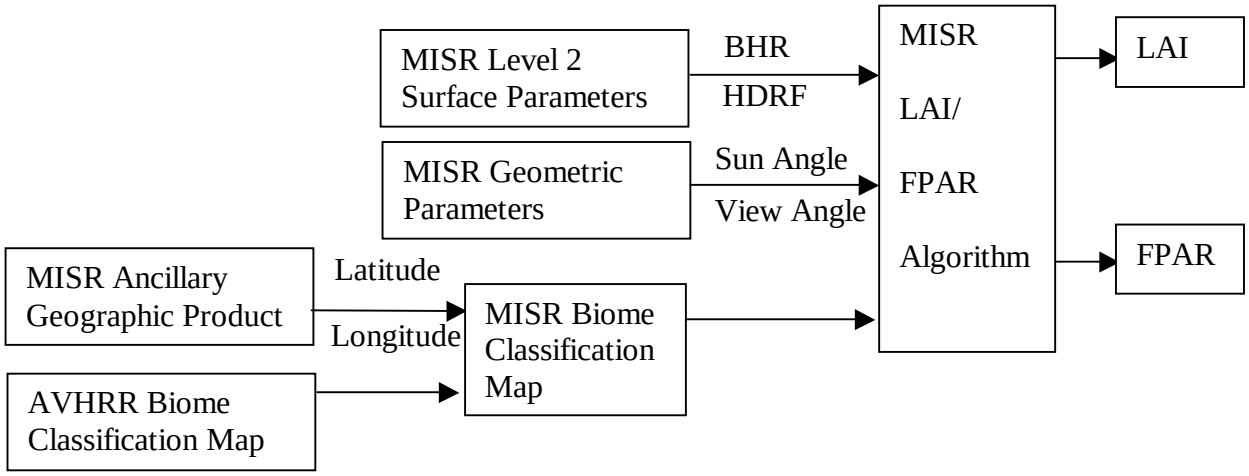

Figure 1. Flow chart of the relationship between MISR LAI/FPAR algorithm and data. Pixel latitude and longitude information from the MISR Ancillary Geographic Product is used to reproject the MODIS biome classification map to the MISR SOM-j projection. The inputs, BHR and BRF from the MISR Level 2 Surface Parameters Product and the sun and view angles from MISR Geometric Parameters Product, are resorted according to biome type. The algorithm is thus executed on a biome basis.

Distributed by the Atmospheric Science Data Center
http://eosweb.larc.nasa.gov

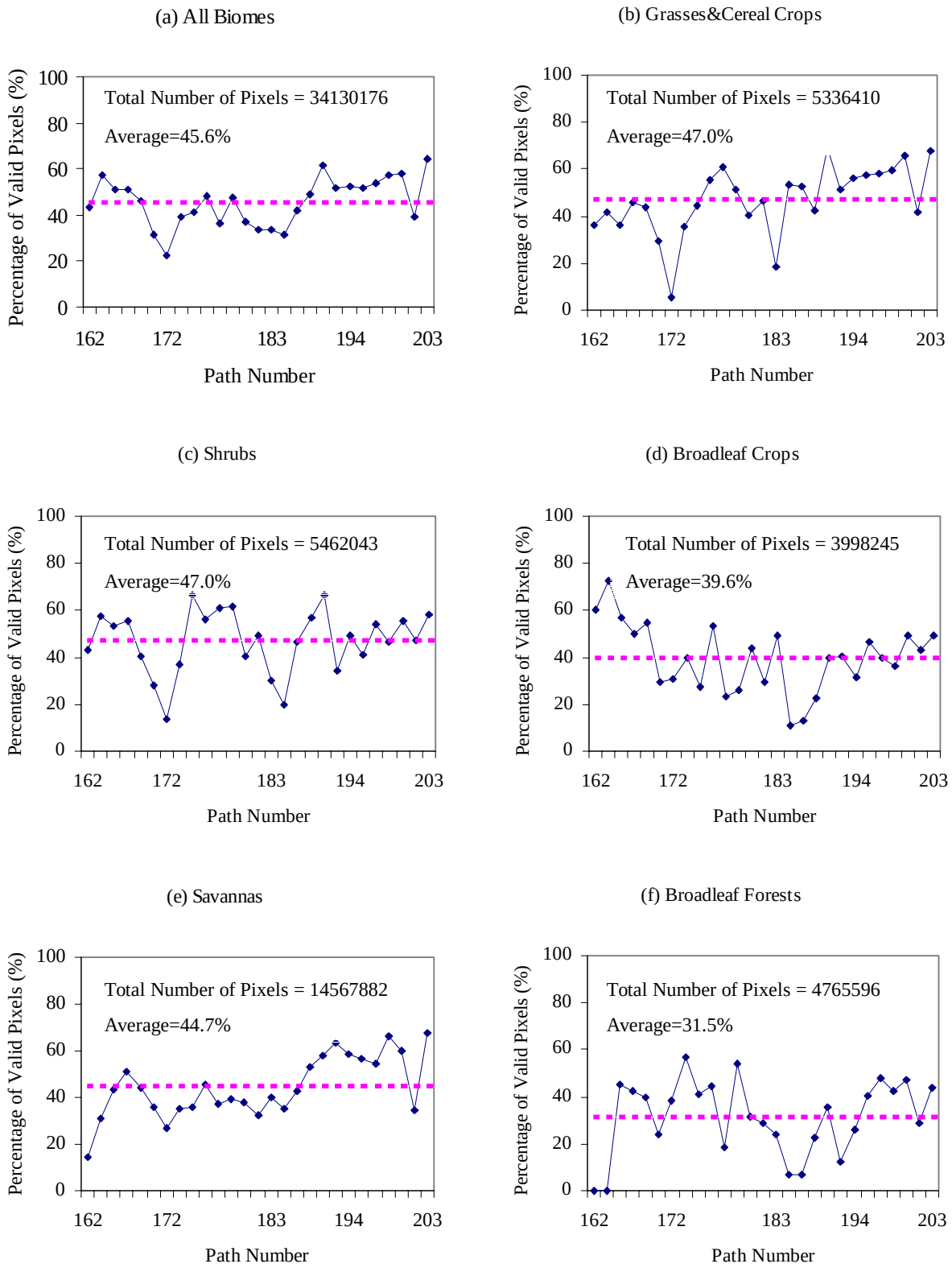

Figure 2. Ratio of valid pixel number to total pixel number, in percentage. (a) All biomes, (b) Grasses and Cereal Crops, (c) Shrubs, (d) Broadleaf Crops, (e) Savannas, (f) Broadleaf Forests. There is no significant presence of needleleaf forests in Africa. The average ratio is shown in these plots as a dashed line. The maximum is for Shrubs (47%), and the minimum is for Broadleaf Forest (31.5%).

Distributed by the Atmospheric Science Data Center
http://eosweb.larc.nasa.gov

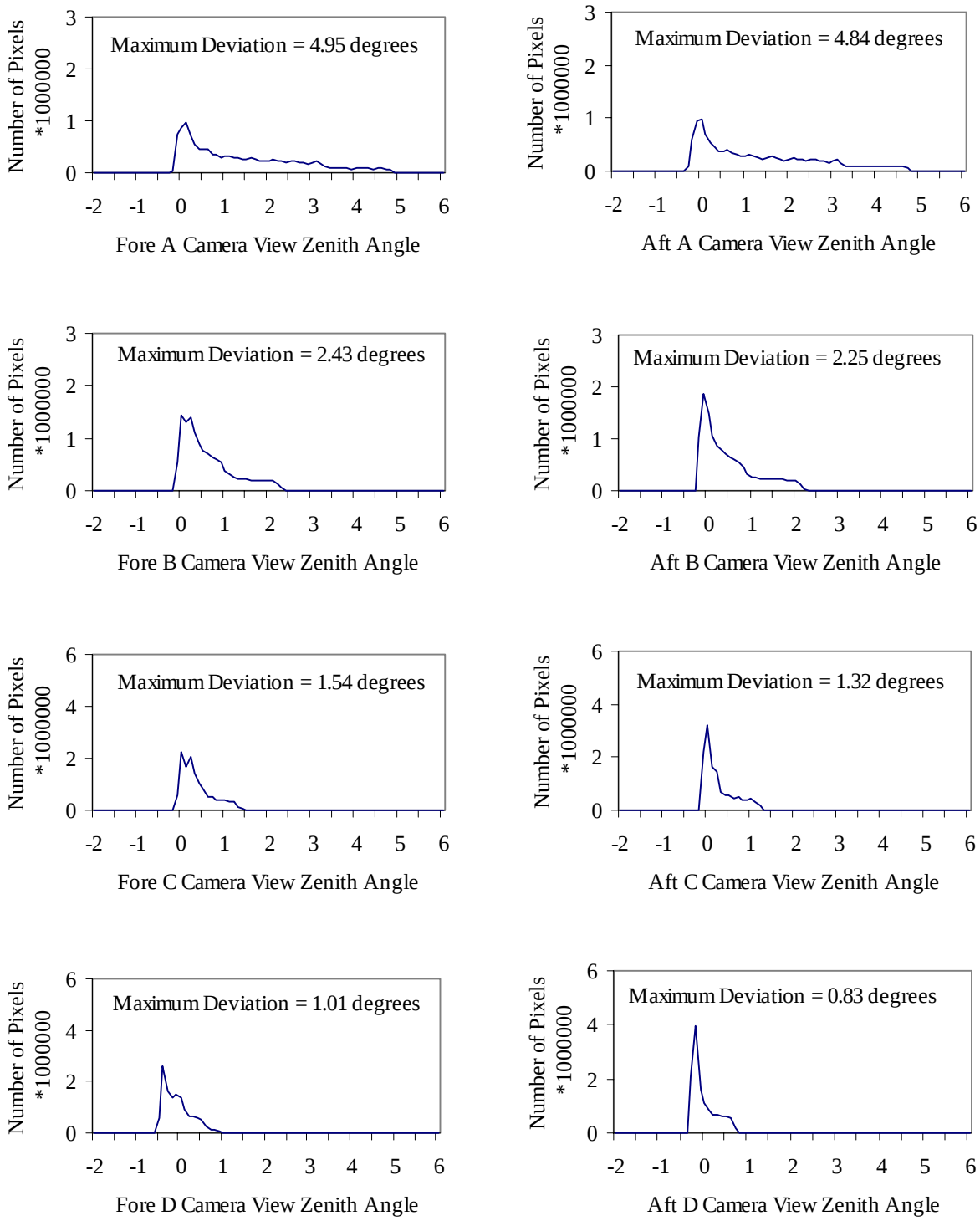

Figure 3. Histograms of the difference between nominal and actual viewing angles. The maximum deviation is labeled for each camera.

Distributed by the Atmospheric Science Data Center
http://eosweb.larc.nasa.gov

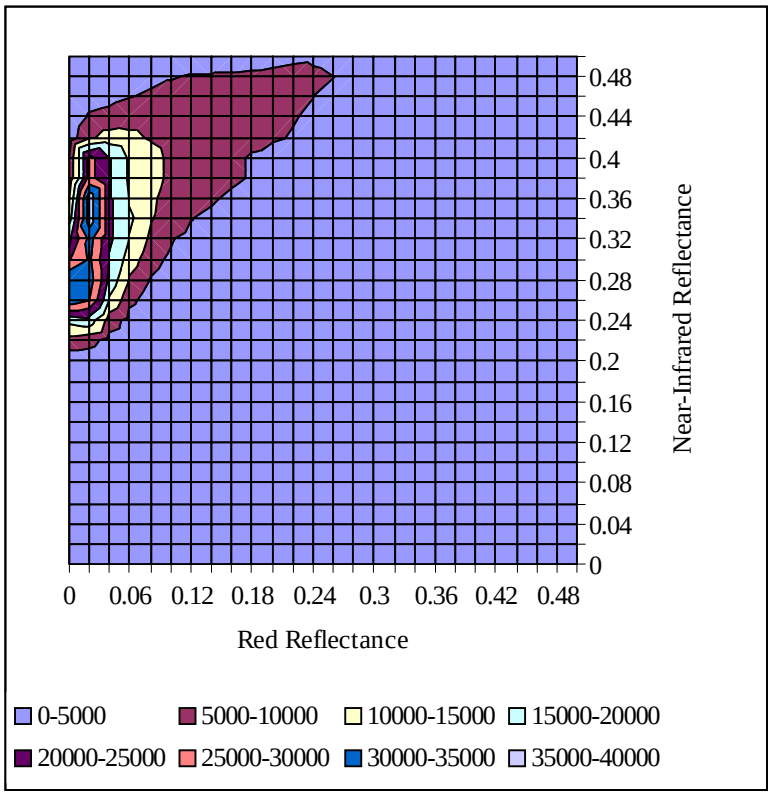

Figure 4a. Distribution of pixel counts in the red and near-infrared DHR space for broadleaf forests biome. Pixels located around data peak (0.02, 0.36), may be interpreted as pixels characteristic of broadleaf forest biome type.

Distributed by the Atmospheric Science Data Center
http://eosweb.larc.nasa.gov

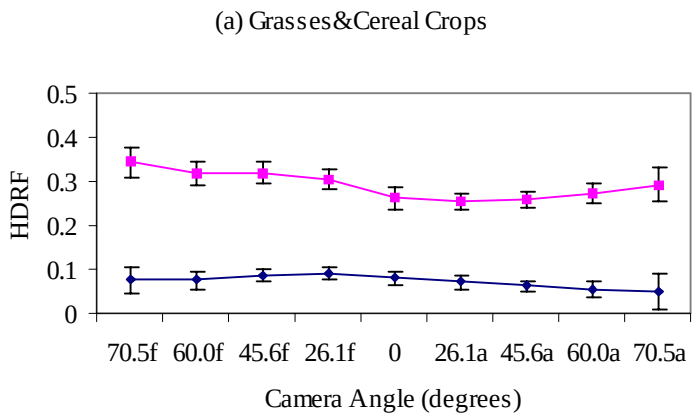

Fig. 4b

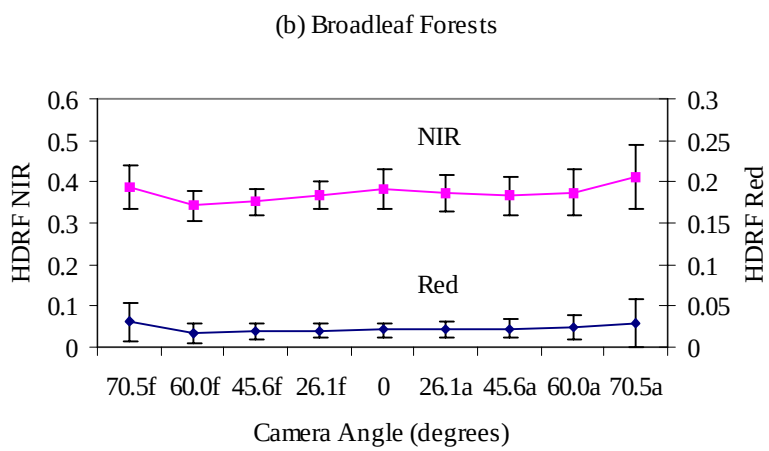

Fig. 4c

Figure 4b and 4c. The mean and standard deviation of HDRFs at red and NIR wavelengths derived from pixels located around the data peak for: (a) Grasses & Cereal Crops, (b) Broadleaf Forests

Distributed by the Atmospheric Science Data Center
http://eosweb.larc.nasa.gov

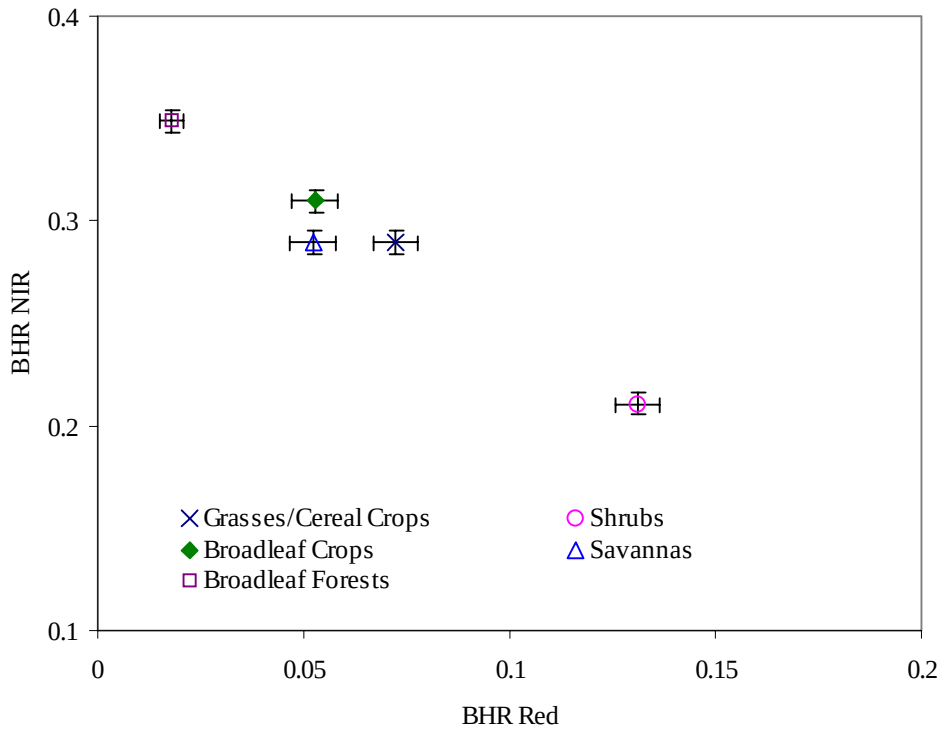

Figure 4d. Mean and standard deviation of MISR BHR values from pixels near the data density maximum (there is no appreciable needleleaf forest presence in Africa).

Distributed by the Atmospheric Science Data Center
http://eosweb.larc.nasa.gov

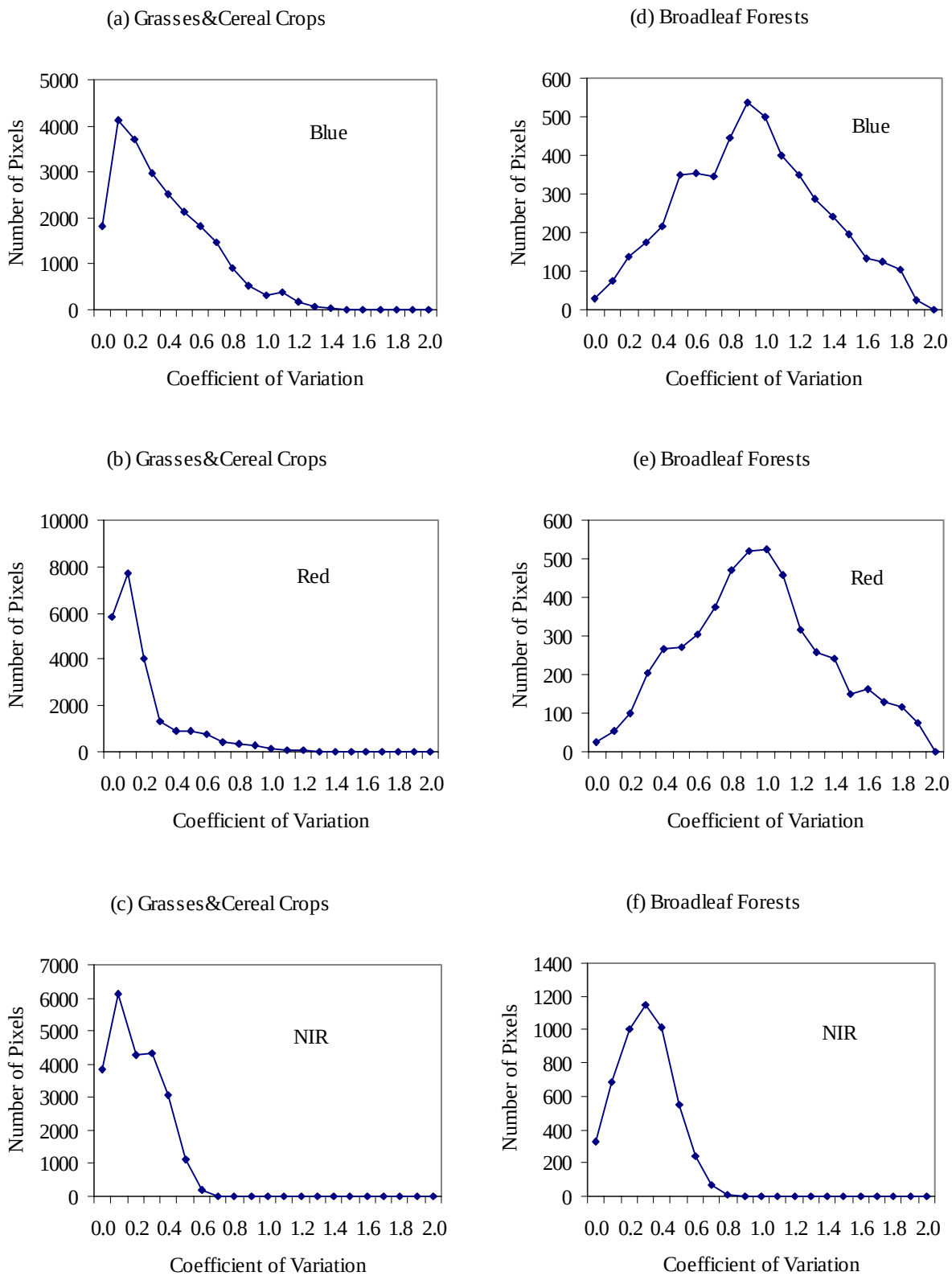

Figure 5. Histogram of Standard Deviation/Mean of data from path 178 for 3 different days, orbit 6393 (Mar 1, 2001), 6626 (Mar 17, 2001) and orbit 6859 (April 2, 2001). Plots are for grasses & cereal crops and broadleaf forests at Blue, Red and NIR bands.

Distributed by the Atmospheric Science Data Center
http://eosweb.larc.nasa.gov

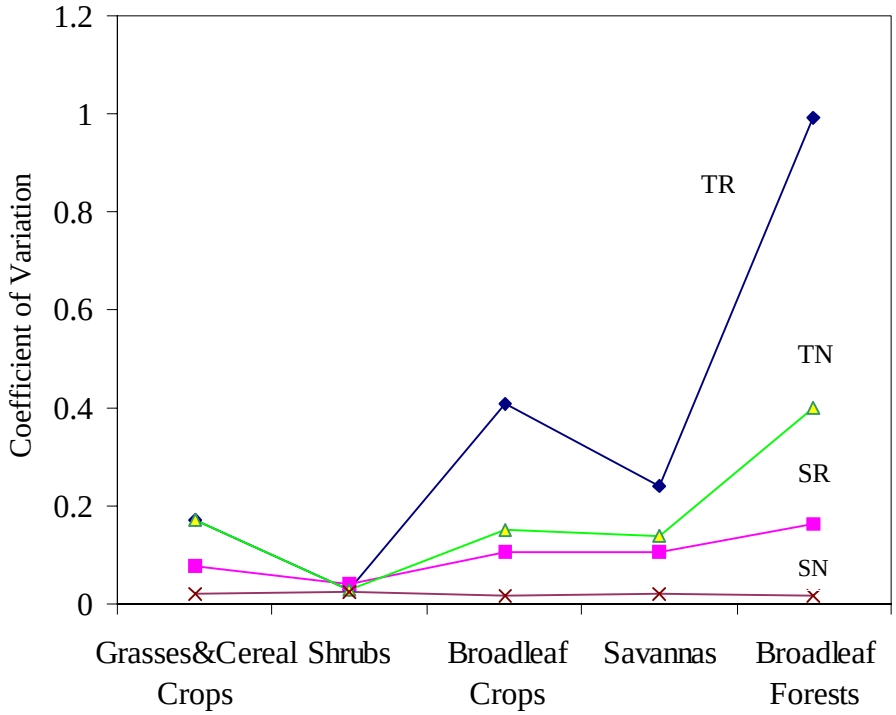

Figure 6. Mean coefficient of variation of DHR at Red and NIR wavelengths derived from spatial and temporal analysis of MISR data. The data described in Figs. 4d and 5 are used to derive spatial and temporal variation in MISR surface reflectance. Labels TN and TR refer to the temporal, and SR and SN refer to the spatial coefficients of variation at Red and NIR spectral bands.

Distributed by the Atmospheric Science Data Center
http://eosweb.larc.nasa.gov

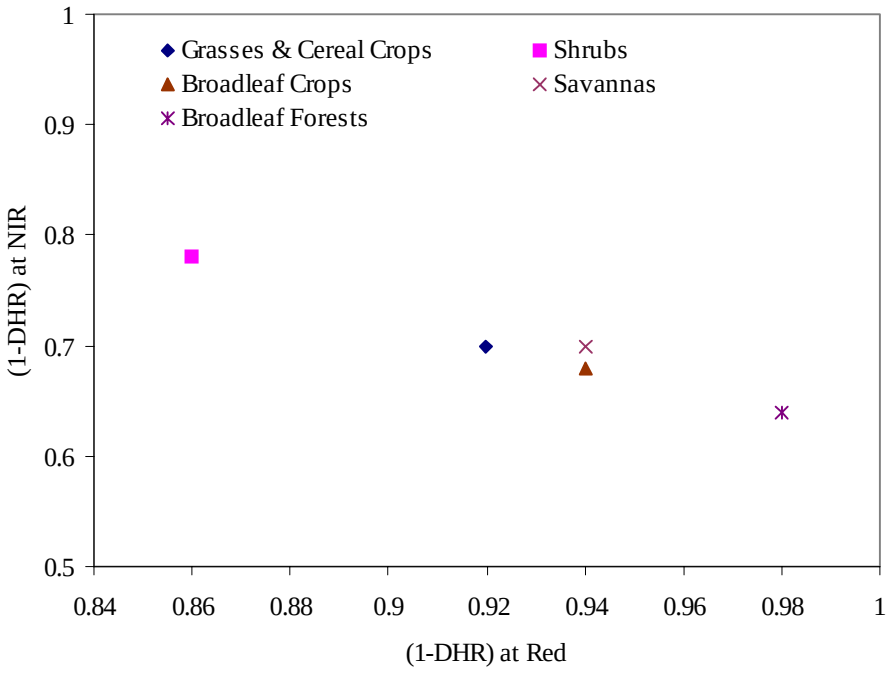

Figure 7a. Fraction of energy, (1-DHR), absorbed by the vegetated surface at Red and NIR wavelengths by different cover types. Pixels located around the data peak (see Fig. 4a) were used to derive values of (1-DHR).

Distributed by the Atmospheric Science Data Center
http://eosweb.larc.nasa.gov

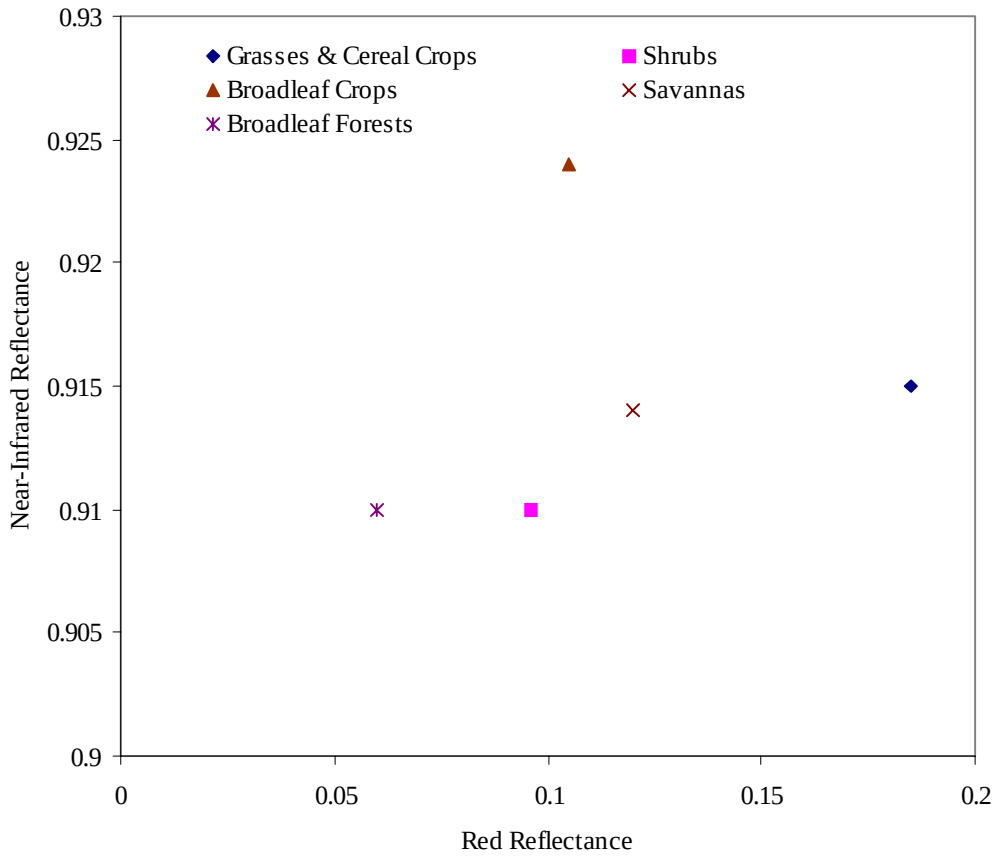

Figure 7b. Adjusted single scattering albedos of different cover types used by the operational MISR LAI/FPAR software.

Distributed by the Atmospheric Science Data Center
http://eosweb.larc.nasa.gov

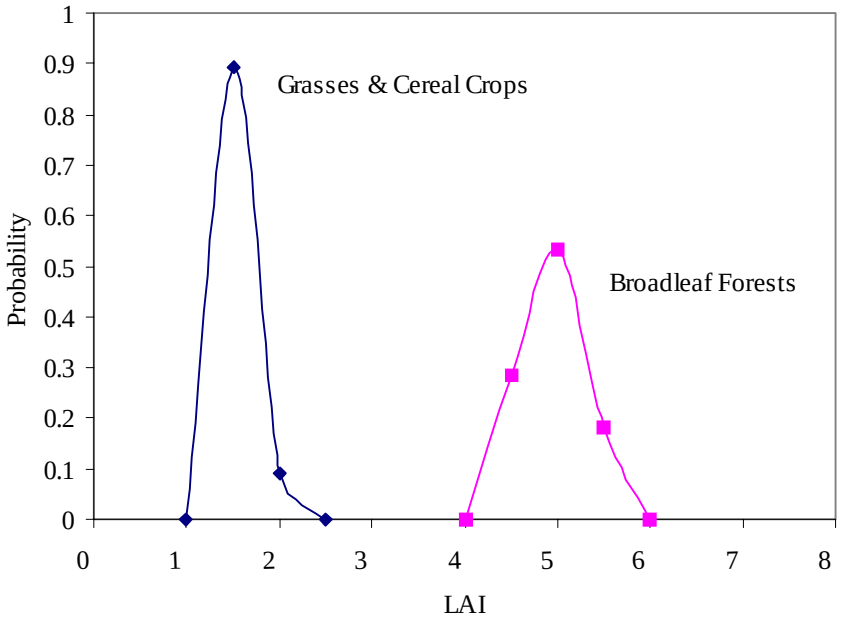

Figure 7c. Histogram of LAI values produced by the MISR algorithm using surface reflectances located around the data peak (see Fig. 4a). Single scattering albedos shown in Fig. 7b were used. Uncertainties in MISR BHRs and BRFs were set to 0.2 based on analysis presented in Figs. 5 to 6. The left curve is for grasses & cereal crops with peak probability at LAI = 1.5 (mean LAI = 1.27) and the right curve is for broadleaf forests with peak probability at LAI = 5.0.

Distributed by the Atmospheric Science Data Center
http://eosweb.larc.nasa.gov

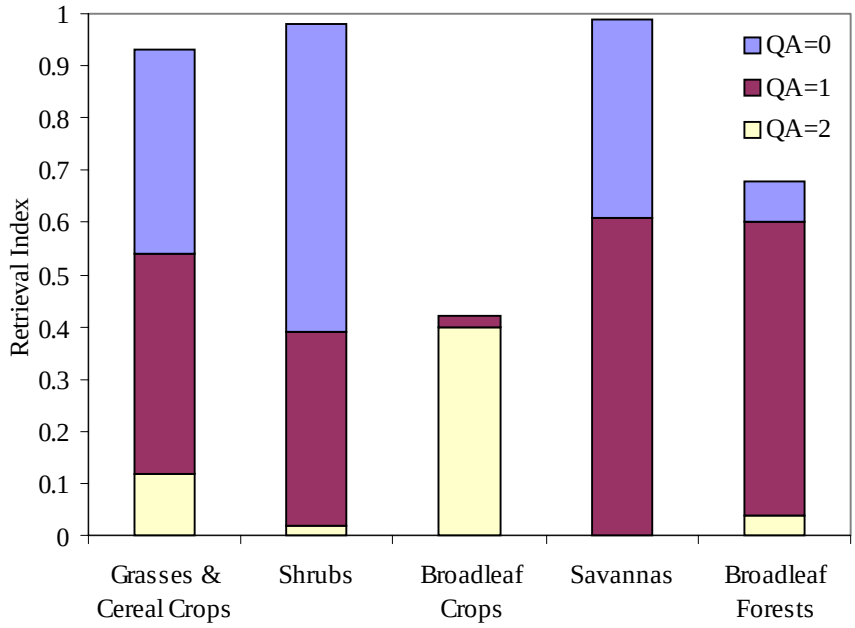

Figure 8a. Retrieval index as a function of biome type and Quality indicator of the Algorithm (QA) for optimal set of relative uncertainties listed in Tables 1 and 2. Pixels located around the data peak and the six-biome classification map were used to derive values of the retrieval index. In this case, the retrieval index is the conditional probability of retrieving LAI value given the biome type.

Distributed by the Atmospheric Science Data Center
http://eosweb.larc.nasa.gov

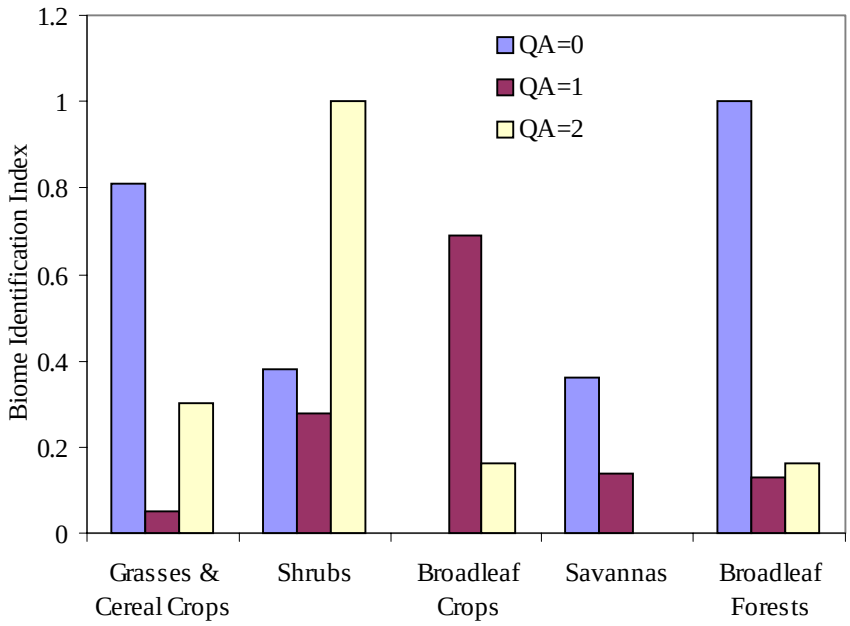

Figure 8b. Biome identification index (BI) as a function of biome type and QA for the optimal set of relative uncertainties. Pixels for which the MISR algorithm retrieved LAI values using the six-biome map and surface reflectance located around data peaks were used to evaluate the BI.

Distributed by the Atmospheric Science Data Center
http://eosweb.larc.nasa.gov

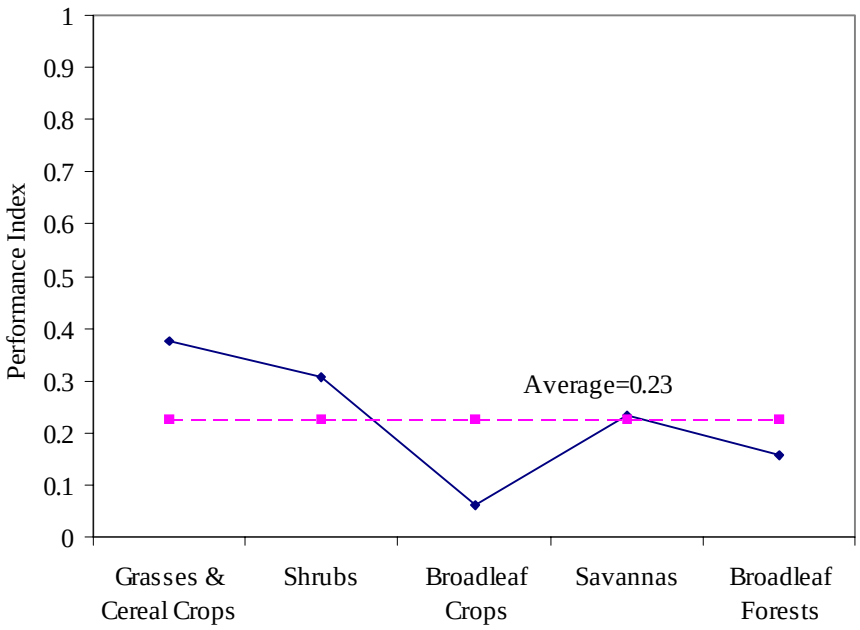

Figure 8c. Performance index (PI) as a function of biome type for optimal set of relative uncertainties.

Distributed by the Atmospheric Science Data Center
http://eosweb.larc.nasa.gov

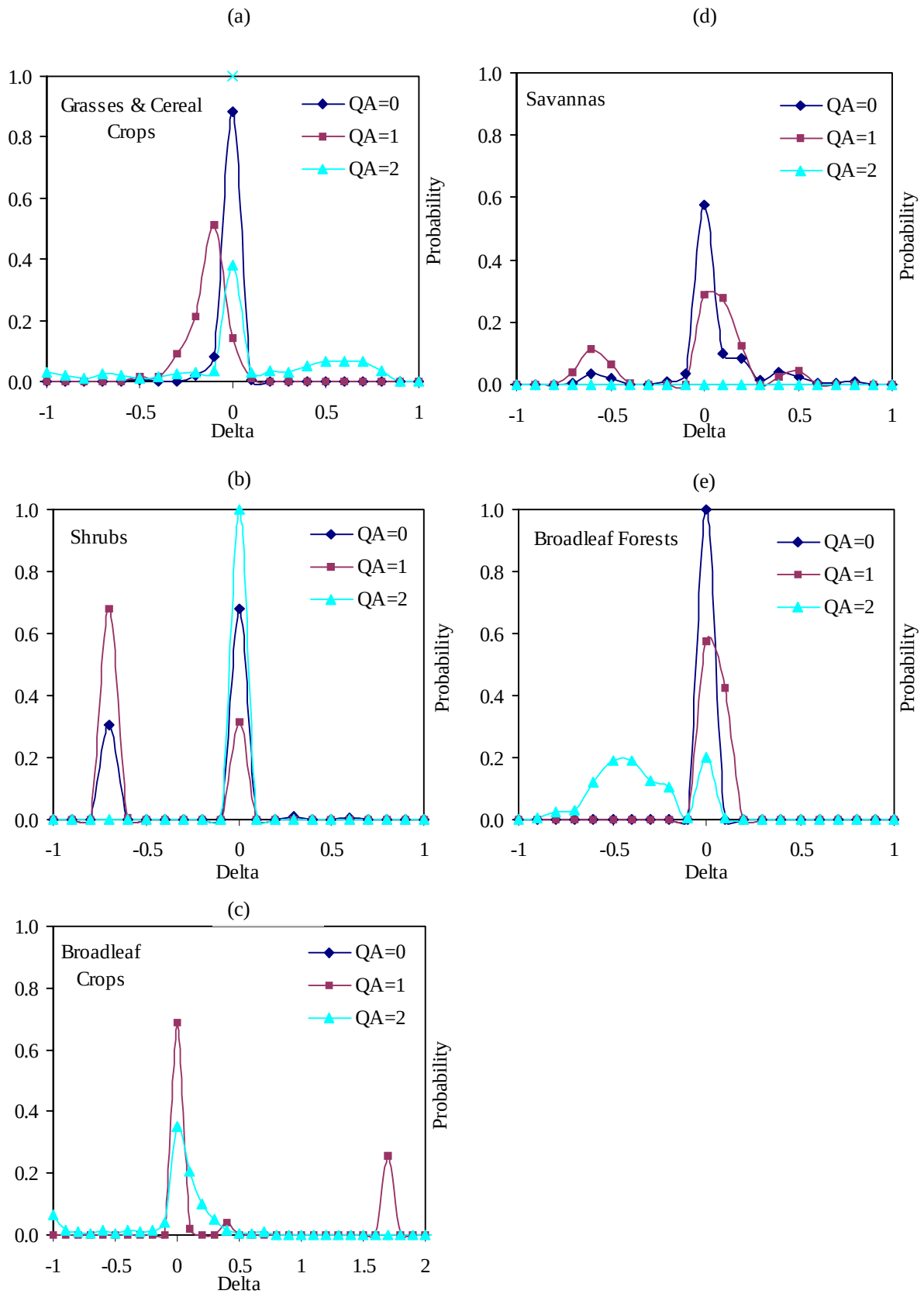

Figure 9. Histograms of the relative difference between reference and retrieved LAI values for different biome type and QA.

Distributed by the Atmospheric Science Data Center
http://eosweb.larc.nasa.gov

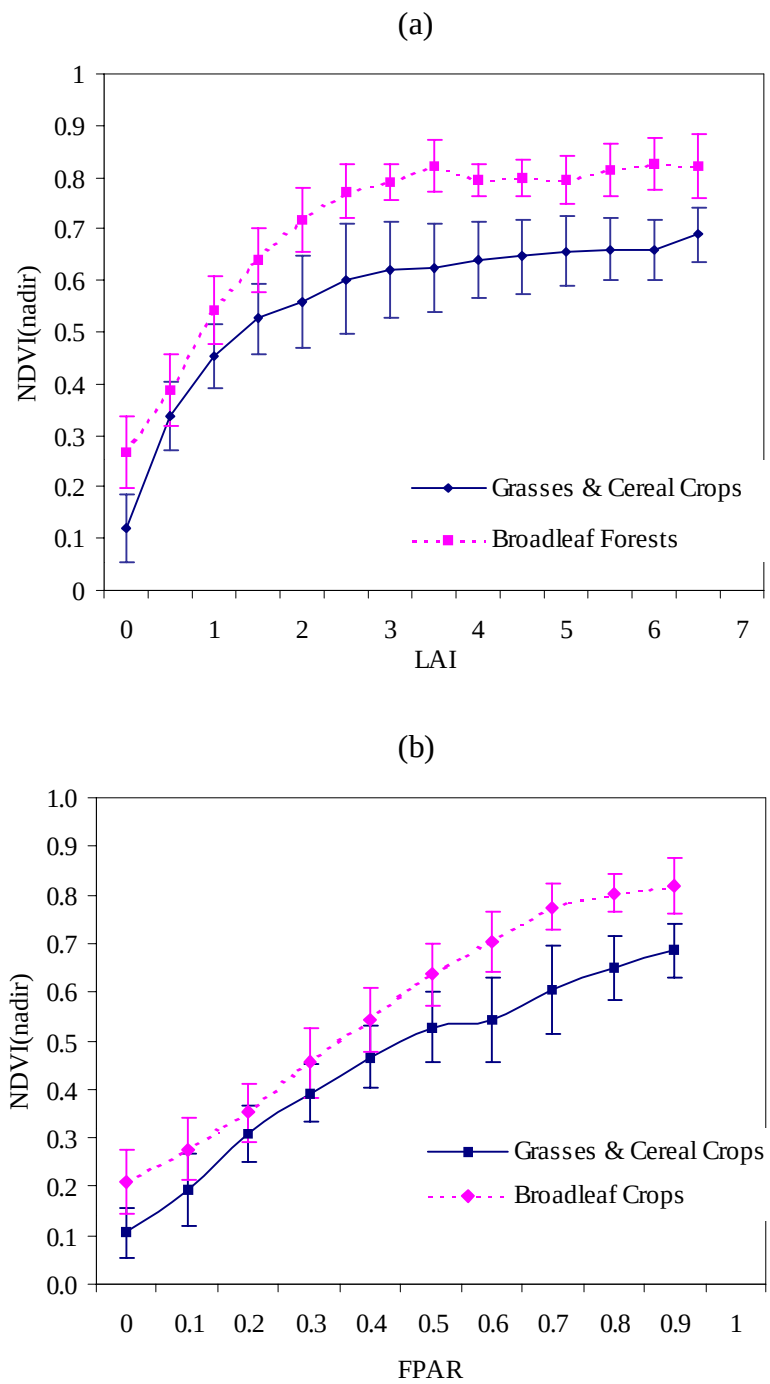

Figure 10. (a) NDVI-LAI and (b) NDVI-FPAR regression curves for grasses and broadleaf forests, based on the MISR data. High quality retrievals (QA=0) were used to derive these curves.

Distributed by the Atmospheric Science Data Center
http://eosweb.larc.nasa.gov

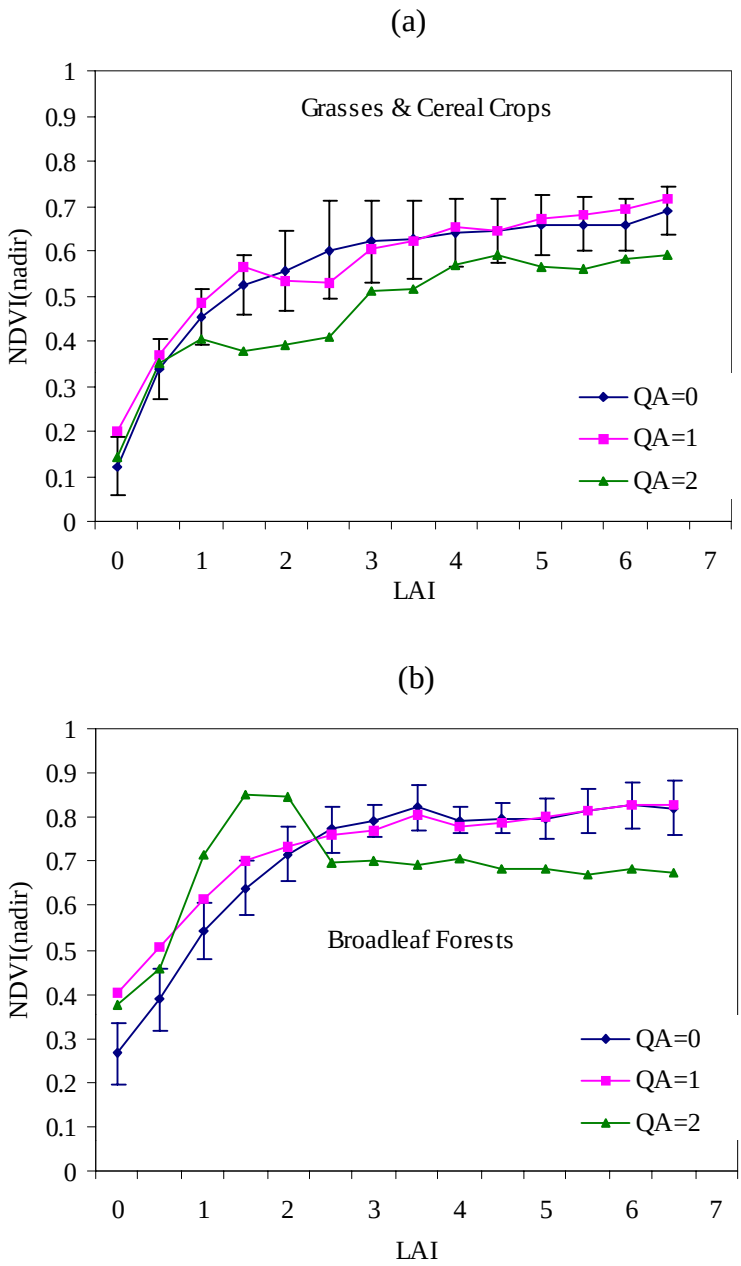

Figure 11. NDVI-LAI regression curves for (a) grasses/cereal crops and (b) broadleaf forests for different values of QA.

Distributed by the Atmospheric Science Data Center
http://eosweb.larc.nasa.gov